MOLECULAR AND CELLULAR BIOLOGY, Mar. 2010, p. 1231–1242 Vol. 30, No. 5
0270-7306/10/$12.00 doi:10.1128/MCB.01269-09


# The ARF-Like GTPase ARFRP1 Is Essential for Lipid Droplet Growth and Is Involved in the Regulation of Lipolysis▽

Angela Hommel,[1] Deike Hesse,[1] Wolfgang Völker,[2] Alexander Jaschke,[1] Markus Moser,[3] Thomas Engel,[2] Matthias Blüher,[4] Claudia Zahn,[1] Alexandra Chadt,[1] Karen Ruschke,[4] Heike Vogel,[1] Reinhart Kluge,[1] Horst Robenek,[2] Hans-Georg Joost,[1] and Annette Schürmann[1]*

*Department of Experimental Diabetology, German Institute of Human Nutrition Potsdam-Rehbruecke, D-14558 Nuthetal, Germany[1]; Leibniz Institute for Arteriosclerosis Research, University of Münster, D-48148 Münster, Germany[2]; Department of Molecular Medicine, Max Planck Institute of Biochemistry, D-82152 Martinsried, Germany[3]; and Department of Medicine, University of Leipzig, D-04103 Leipzig, Germany[4]*

Received 21 September 2009/Returned for modification 17 October 2009/Accepted 16 December 2009

**ADP-ribosylation factor (ARF)-related protein 1 (ARFRP1) is a GTPase regulating protein trafficking between intracellular organelles. Here we show that mice lacking *Arfrp1* in adipocytes (*Arfrp1*$^{ad-/-}$) are lipodystrophic due to a defective lipid droplet formation in adipose cells. Ratios of mono-, di-, and triacylglycerol, as well as the fatty acid composition of triglycerides, were unaltered. Lipid droplets of brown adipocytes of *Arfrp1*$^{ad-/-}$ mice were considerably smaller and exhibited ultrastructural alterations, such as a disturbed interaction of small lipid-loaded particles with the larger droplets, suggesting that ARFRP1 mediates the transfer of newly formed small lipid particles to the large storage droplets. SNAP23 (synaptosomal-associated protein of 23 kDa) associated with small lipid droplets of control adipocytes but was located predominantly in the cytosol of *Arfrp1*$^{ad-/-}$ adipocytes, suggesting that lipid droplet growth is defective in *Arfrp1*$^{ad-/-}$ mice. In addition, levels of phosphorylated hormone-sensitive lipase (HSL) were elevated, and association of adipocyte triglyceride lipase (ATGL) with lipid droplets was enhanced in brown adipose tissue from *Arfrp1*$^{ad-/-}$ mice. Accordingly, basal lipolysis was increased after knockdown of *Arfrp1* in 3T3-L1 adipocytes. The data indicate that disruption of ARFRP1 prevents the normal enlargement of lipid droplets and produces an activation of lipolysis.**

The GTPase ADP-ribosylation factor (ARF)-related protein 1 (ARFRP1) (34) is a member of the family of ARFs that operate as GTP-dependent molecular switches in the regulation of intracellular protein traffic and in Golgi function (18, 19). ARFRP1 in 3T3-L1 adipocytes was identified in a PCR-based screen of differentially expressed transcripts. In addition, it is expressed in brown adipose tissue, liver, kidney, intestine, and lung (34). GTP-bound ARFRP1 specifically binds the guanine nucleotide exchange factor of ARF1, mSec7-1/cytohesin, and inhibits ARF-controlled pathways (35). ARFRP1 is associated with *trans*-Golgi membranes (47) and controls the recruitment of proteins such as ARL1 (ARF-like 1) and its effector golgin-245 to *trans*-Golgi membranes (31, 39, 47). Due to defective E-cadherin targeting and adhesion defects, conventional *Arfrp1*$^{-/-}$ embryos die during early gastrulation (27, 48).

Adipose tissue plays an important role for energy homeostasis. Adipocytes of brown adipose tissue (BAT) generate heat via mitochondrial uncoupling of lipid oxidation (37). White adipose tissue (WAT) is the major organ for regulated storage of triglycerides, which are used as metabolic energy to be mobilized during fasting and extended exercise (8, 41). Triglycerides are stored in lipid droplets (LDs) formed at membranes of the endoplasmic reticulum (ER), and their assembly depends on the rate of triglyceride synthesis (24). In addition, droplets increase in size by fusion which is catalyzed by the SNAREs, SNAP23, syntaxin-5, and VAMP4 (6, 21, 29).

LDs are surrounded by a phospholipid monolayer which binds a number of proteins, particularly the PAT family proteins *p*erilipin, *A*DRP (adipocyte differentiation-related protein [adipophilin]), and *T*IP47 (tail-interacting protein of 47 kDa) and are recognized as dynamic organelles (3, 7, 9, 29, 32). In addition, proteins involved in sorting and trafficking events in the cell and interacting with other organelles also associate with LDs (22, 29, 30).

The high expression of ARFRP1 in adipose tissue suggested that the GTPase plays an important role in the regulation of adipocyte-specific processes. Thus, in order to define this role, we generated and characterized mice with a fat cell-specific deletion of *Arfrp1*. We found that triglyceride storage was almost abolished, LDs were smaller, and lipolysis was enhanced. Furthermore, ultrastructural analysis indicated that ARFRP1 controls the interaction of small lipid-loaded particles with storage LDs.

## MATERIALS AND METHODS

**Generation of *Arfrp1*$^{ad-/-}$ mice.** For tissue-specific disruption of *Arfrp1* (*Arfrp1*$^{ad-/-}$ mice), *Arfrp1*$^{flox/flox}$ mice (48) were intercrossed with transgenic mice expressing the Cre recombinase under the control of the *Fabp4*/*aP2* promoter/enhancer (*aP2-Cre*) (17). PCR-based genotyping of *Arfrp1*$^{ad-/-}$ mice was performed with the following primers: *aP2-Cre*, 5′-TCTCACGTACTGACGGTGG-3′ and 5′-ACCAGCTTGCATGATCTCC-3′; for the upstream 5′ *loxP* site,

* Corresponding author. Mailing address: Department of Experimental Diabetology, German Institute of Human Nutrition Potsdam-Rehbruecke, Arthur-Scheunert-Allee 114-116, D-14558 Nuthetal, Germany. Phone: (49) 33200-88368. Fax: (49) 33200-88334. E-mail: schuermann@dife.de.

▽ Published ahead of print on 28 December 2009.

5′-CAGGGTCAGGGATTTTAACAG-3′; and for the downstream 3′ *loxP* site, 5′-GAAAGCAACTTGGGAACCTG-3′. Deletion of exons 2 to 4 of *Arfrp1* was verified as described previously (48). The animals were housed in a controlled environment (20 ± 2°C, 12 h/12 h of a light/dark cycle) and had free access to water and standard chow diet. All animal experiments were approved by the ethics committee of the Ministry of Agriculture, Nutrition, and Forestry (State of Brandenburg, Germany).

**Antibodies.** We used the polyclonal antiserum against recombinant GST-ARFRP1 as described previously (32, 44). For Western blot analysis of adiponectin, we used polyclonal antiadiponectin antibody (ab3455; Abcam) in a dilution of 1:500. Polyclonal antiserum against GLUT4 was described previously (32) and used for immunohistochemistry in a dilution of 1:1,000. Polyclonal antiserum against FATP1 was described previously (43) and used in a dilution of 1:800. Anti-UCP1 antiserum (Abcam, Cambridge, United Kingdom) was used in a dilution of 1:1,000. Anti-SNAP23 was purchased from Abcam and used in a dilution of 1:500 for immunohistochemistry and for Western blotting in a dilution of 1:1,000. Antisera against perilipin, ADRP (Progen Biotechnik GmbH, Wieblingen, Germany), and TIP47 (AnaSpec, San Jose, CA) were used for immunohistochemistry in a dilution of 1:5,000, 1:250, and 1:100, respectively, and for Western blotting in a dilution of 1:2,000 with perilipin. The anti-HSL and anti-pHSL antibodies were purchased from Cell Signaling (Boston, MA) and used in a dilution of 1:1,000 for Western blotting and of 1:800 for cytochemistry. Anti-Cav1 antiserum (Serotec, Oxford, United Kingdom) was used in a dilution of 1:2,000 and anti-Cav2 antiserum (BD Transduction Laboratories, Franklin Lakes, NJ) in a 1:1,000 dilution. Anti-Rab18 from Abcam was used in a dilution of 1:100 for immunohistochemistry. Affinity-purified polyclonal antiserum against recombinant ARL1 (E6P3) was described previously (47) and used in a dilution of 1:800. An Alexa Fluor 546 F(ab′)2 fragment of goat anti-rabbit IgG (H+L) and Alexa Fluor 488 F(ab′)2 fragment of goat anti-mouse IgG (H+L) (Molecular Probes, Eugene, OR) were used in a dilution of 1:800 as secondary antibodies. An antibody against glyceraldehyde phosphate dehydrogenase (GAPDH; Ambion, Austin, TX) was used in a dilution of 1:20,000 as a loading control.

**Characterization of mice.** Quantitative real-time PCR, detection of body fat content, and plasma and histochemical analyses were performed as described previously (10). For the determination of *Arfrp1* mRNA levels and to analyze expression of fat-specific genes, the following TaqMan gene expression assays (Applied Biosystems) were used: *Arfrp1* E2_E3 (Mm01220415_g1), *Slc2a4*/GLUT4 (Mm00436615_m1), *Pparg*/PPARγ (Mm00440945_m1), *Fabp4*/*aP2* (Mm00495574), *Ucp1* (Mm00494069_m1), *Cebpa*/C/EBPα (Mm00514283_s1), *Hsl* (Mm00495359_m1), *Atgl* (Mm00503040_m1), *Fasn* (Mm00662319_m1), and *Fatp1* (Mm00449511_m1). Data were normalized as described previously (10), whereas a β-actin expression assay (Mm00607939_s1) was used as an endogenous control.

**Body composition.** For the examination of body fat content, a nuclear resonance spectrometer (Bruker minispec NMR analyzer mq10, Bruker Optics, Houston, TX) was used.

**Plasma analysis.** Levels of plasma leptin were examined by using a rat leptin enzyme-linked immunosorbent (ELISA) kit (Crystal Chem Inc., Illinois).

**Determination of lipids and fatty acids in BAT.** Total neutral lipids were extracted from 1 to 10 mg BAT of 7-day-old $Arfrp1^{flox/flox}$ and $Arfrp1^{ad-/-}$ mice by a method described previously (14). Triglycerides were measured with an enzymatic method (Randox Laboratories, Crumlin, United Kingdom).

For determination of mono-, di-, and triacylglycerol, total lipids of BAT were extracted according to the procedure of Folch et al. (13). Samples were separated on a 250- by 4.0-mm LiChrospher 100 Diol 5-μm column by high-performance liquid chromatography (HPLC) in a way similar to that described by Butovich et al. (11), except using the HPA solvent composition and a Kontron HPLC system equipped with a diode array detector set at a 206-nm wavelength and 10-nm band pass for detection. For determination of the fatty acid composition of total lipids, we used a protocol described previously (20).

**Thermographic monitoring of body temperature.** The high-performance noncontact thermometer (FLIR Systems i 50; PK Elektronik Poppe GmbH, Velten, Germany) was set up according to the manufacturer's instructions. Temperatures of individual mice were monitored until a stable reading was achieved, with the unit held 5 cm above the mouse.

**Electron microscopy.** Samples of BAT from 7-day-old $Arfrp1^{flox/flox}$ and $Arfrp1^{ad-/-}$ mice were used for ultrastructural stainings as described previously (36). Ultrathin sections were investigated with a transmission electron microscope (Philips EM201) equipped with a digital imaging system (DITABIS, Pforzheim, Germany).

**Preparation of total membranes and cytosol from BAT.** Samples of BAT (~10 mg) from 7-day-old $Arfrp1^{flox/flox}$ and $Arfrp1^{ad-/-}$ mice were homogenized in a small volume (50 to 100 μl) and centrifuged at 200,000 × *g* for 75 min (4°C). The membrane pellet (P) and the supernatant (SN) were used for Western blot analysis.

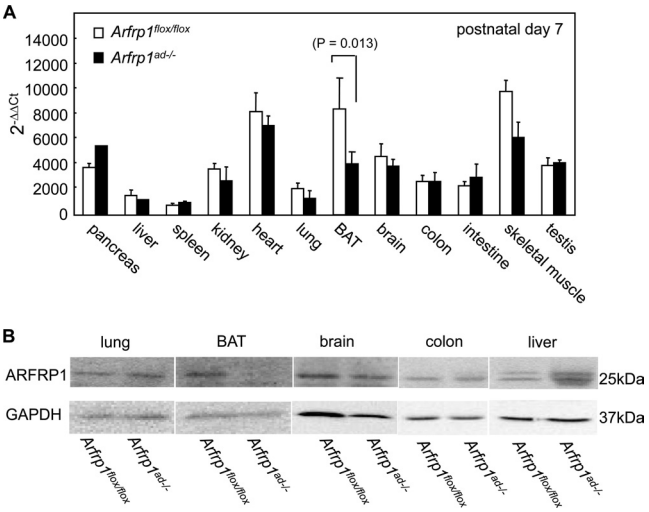


FIG. 1. Conditional deletion of *Arfrp1* in adipose tissue. (A) *Arfrp1* mRNA levels in the indicated tissues of $Arfrp1^{flox/flox}$ and $Arfrp1^{ad-/-}$ mice at the age of 7 days were detected by quantitative RT-PCR as described in Materials and Methods. No white adipose tissue could be collected from $Arfrp1^{ad-/-}$ mice without contamination from adjacent tissues. Values are means + standard errors of the mean (SEM) of 9 to 12 animals per group. Ct, threshold cycle. (B) ARFRP1 protein levels of $Arfrp1^{flox/flox}$ and $Arfrp1^{ad-/-}$ mice at the age of 14 days were detected by Western blotting with an ARFRP1-specific antibody.

**siRNA-mediated knockdown of *Arfrp1* in 3T3-L1 cells.** For downregulation of mature *Arfrp1* 3T3-L1 adipocytes ($5 \times 10^6$ cells/electroporation) were electroporated with the Bio-Rad Gene Pulser II with settings of 170 V and 960 microfarads with 20 nmol *Arfrp1*-specific small interfering RNA (siRNA) (5′-GACUGUACCU GUAAGAUUGUU-3′). For control experiments, cells were electroporated with 20 nmol scrambled siRNA (5′-GACUGUACGUGAUAGAUUGUU-3′). After electroporation, cells were immediately mixed with fresh medium before being reseeded onto multiple-well plates or plated on glass coverslips.

**Detection of palmitate uptake and lipolysis.** Seventy-two h after electroporation of 3T3-L1 adipocytes with siRNA, basal and insulin-stimulated fatty acid uptake was assayed by incubation with 0.5 μCi/ml [1-$^{14}$C]-palmitic acid at 37°C for 20 min as described previously (12). Lipolysis was measured as previously described (5).

**Deletion of *Arfrp1* in mouse embryonic fibroblasts.** Mouse embryonic fibroblasts (MEFs) isolated from $Arfrp1^{+/+}$ and $Arfrp1^{flox/flox}$ embryos and grown (80% confluent) on coverslips were infected with Cre adenovirus (multiplicity of infection [MOI] of 500; Vector Biolabs, Philadelphia, PA) and subsequently incubated with 2 mM oleate for 48 h.

## RESULTS

**Adipose tissue-specific deletion of *Arfrp1*.** For adipose tissue-specific disruption of *Arfrp1*, $Arfrp1^{flox/flox}$ mice (48) were crossed with transgenic mice expressing the Cre-recombinase under the control of a promoter fragment of the *Fabp4*/*aP2* gene in both brown and white adipose tissues (*aP2-Cre*) (17).

Quantitative real-time (qRT)-PCR and Western blot analysis indicated successful disruption of *Arfrp1* in BAT (statistically significant reduction of mRNA levels by 59.4 ± 12.6%; $P = 0.013$) but not in other tissues of $Arfrp1^{ad-/-}$ mice (Fig. 1).

**$Arfrp1^{ad-/-}$ mice exhibit a lipodystrophic phenotype and a defect in thermogenesis.** $Arfrp1^{ad-/-}$ mice were of normal size before and at birth and were indistinguishable from $Arfrp1^{flox/flox}$ littermates. However, during the first days of

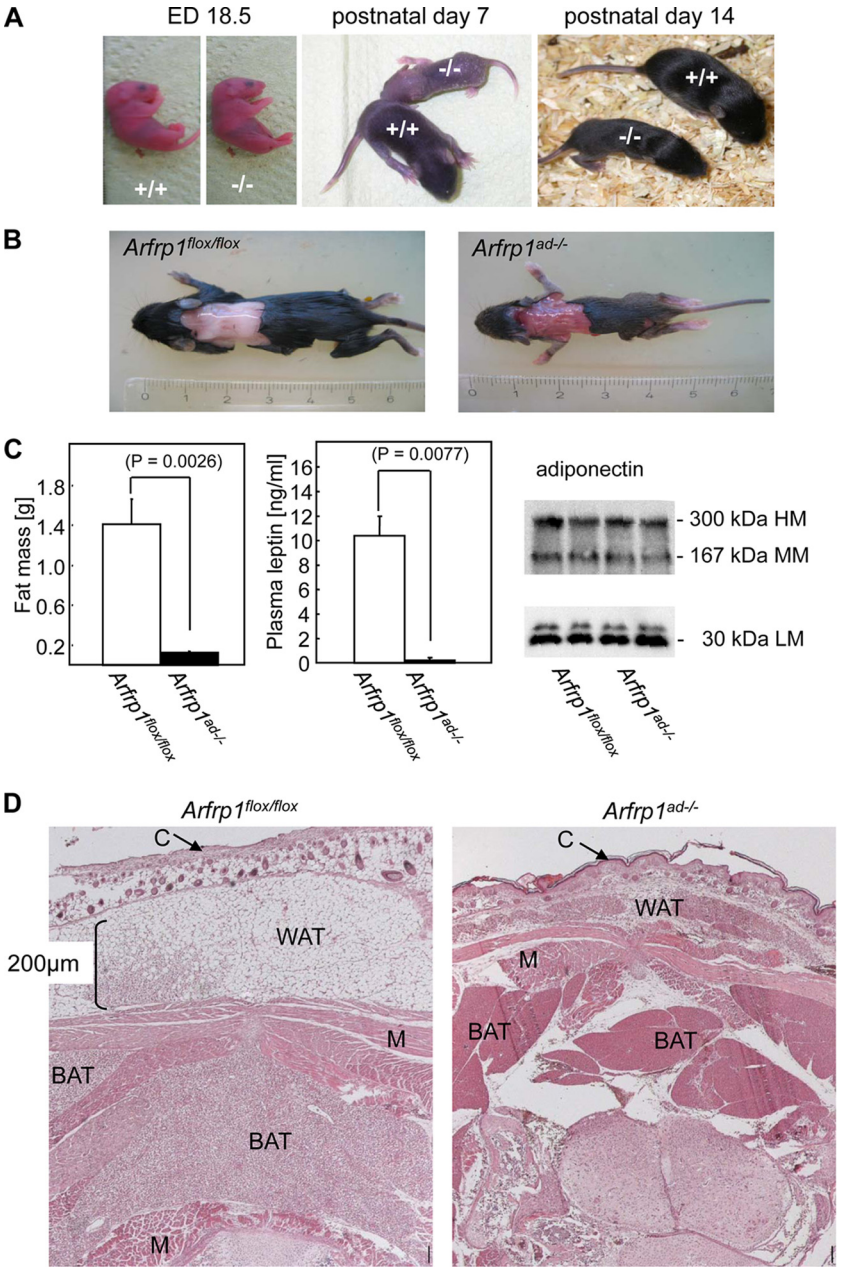


FIG. 2. Postnatal growth retardation and lack of triglyceride stores in white and brown adipocytes. (A) Photographs of *Arfrp1*$^{flox/flox}$ (+/+) and *Arfrp1*$^{ad-/-}$ (−/−) embryos (embryonic day 18.5) and mice at the age of 7 and 14 days. (B) Dorsal view of *Arfrp1*$^{flox/flox}$ and *Arfrp1*$^{ad-/-}$ littermates at the age of 14 days after removal of the skin. (C) Reduced fat mass (left) and plasma leptin (middle) levels and no alteration in adiponectin levels (right) in 14-day-old *Arfrp1*$^{ad-/-}$ mice. HM, high molecular mass; MM, medium molecular mass; LM, low molecular mass. (D) Transverse sections at the level of the neck were obtained from 2-day-old *Arfrp1*$^{flox/flox}$ and *Arfrp1*$^{ad-/-}$ littermates and stained with hematoxylin-eosin (HE). C, cutis; M, muscle.

life, *Arfrp1*$^{ad-/-}$ mice showed a marked growth retardation (Fig. 2A) and a reduced survival rate (about 30%) in comparison to *Arfrp1*$^{flox/flox}$ mice.

No subcutaneous (Fig. 2B) or gonadal (data not shown) WAT was visible in *Arfrp1*$^{ad-/-}$ mice at the age of 14 days. This observation was confirmed by measurement of total fat mass by nuclear magnetic resonance spectrometry. Fourteen-day-old *Arfrp1*$^{flox/flox}$ mice with a mean body weight of 8.1 ± 1.1 g had 1.4 ± 0.5 g (14%) body fat, whereas *Arfrp1*$^{ad-/-}$ mice with a mean body weight of 3.5 ± 0.9 g had a fat mass of only 0.1 ± 0.06 g (3%) (Fig. 2C, left). Circulating leptin was almost undetectable in 14-day-old *Arfrp1*$^{ad-/-}$ mice (Fig. 2C, middle), but no changes in adiponectin levels as detected by ELISA (10.19 ± 0.9 μg/ml in *Arfrp1*$^{flox/flox}$ mice and 9.03 ± 2.0 μg/ml in *Arfrp1*$^{ad-/-}$ mice) or in the pattern of different higher-order complexes of adiponectin as detected by Western blotting were visible in the plasma samples of *Arfrp1*$^{ad-/-}$ mice (Fig. 2C, right).

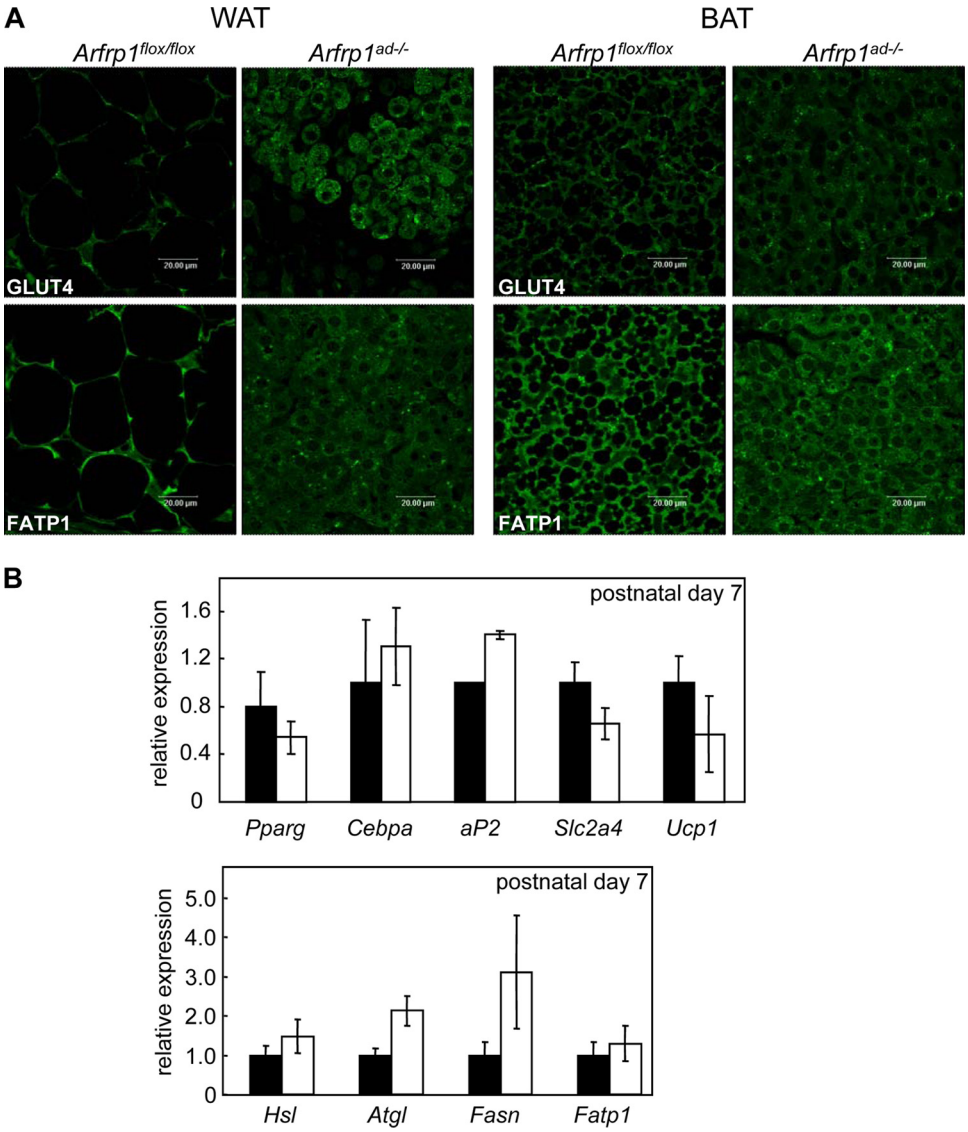


FIG. 3. Expression analysis of adipocyte-specific genes in adipose tissues from *Arfrp1*$^{flox/flox}$ and *Arfrp1*$^{ad-/-}$ littermates. (A) Immunohistochemical detection of GLUT4 and FATP1 in WAT and BAT of 2-day-old *Arfrp1*$^{flox/flox}$ and *Arfrp1*$^{ad-/-}$ mice. (B) Quantitative RT-PCR for the indicated mRNAs in BAT at postnatal day 7. Values are mean ± SEM of 7 to 8 animals per group.

Histology of transverse sections of the neck indicated that control mice had abundant subcutaneous WAT and interscapular BAT at day 2. In contrast, WAT was nearly absent in newborn *Arfrp1*$^{ad-/-}$ mice (Fig. 2D), and the size of BAT was markedly reduced (see below and also Fig. 4A, left). Interestingly, the dwarfish adipose tissues of *Arfrp1*$^{ad-/-}$ mice express typical adipocyte markers, such as the glucose transporter GLUT4 and the fatty acid transporter FATP1 (Fig. 3A). Since the amount of WAT in *Arfrp1*$^{ad-/-}$ mice was very low, we performed the following studies only with BAT, which could be isolated as a small fat pad. qRT-PCR analysis of transcripts that appear at different stages of adipocyte differentiation demonstrated that expression of *Pparg*, *Cebpa*, *Fabp4*/*aP2*, *Slc2a4*, and *Ucp1* was not significantly different in BAT of 7-day-old *Arfrp1*$^{flox/flox}$ and *Arfrp1*$^{ad-/-}$ mice. mRNA expression of enzymes involved in fatty acid transport (*Fatp1*), fatty acid synthesis (*Fasn*), and lipolysis (hormone-sensitive lipase, *Hsl*; and adipose triglyceride lipase, *Atgl*) were not significantly reduced in BAT of *Arfrp1*$^{ad-/-}$ mice; mRNA of *Atgl* and *Fasn* showed a tendency toward increased expression in the null mutants (Fig. 3B). The size of BAT of 7-day-old *Arfrp1*$^{ad-/-}$ mice was significantly reduced (*Arfrp1*$^{flox/flox}$, 24.18 ± 12.2; and *Arfrp1*$^{ad-/-}$, 13.18 ± 11.1 mg; $P = 0.0009$) (Fig. 4A). In addition, cells of the BAT of *Arfrp1*$^{ad-/-}$ mice were much smaller than those of *Arfrp1*$^{flox/flox}$ mice and accumulated only few LDs, as detected by oil Red O staining (Fig. 4A).

As BAT is responsible for thermogenesis, we measured body temperature of 7-day-old mice by infrared thermometry and detection of axillary temperature. In *Arfrp1*$^{flox/flox}$ mice, axillary temperatures were in the range between 30.1 and 33.9°C and in *Arfrp1*$^{ad-/-}$ mice between 25.5 and 32.2°C; hence, the mean body temperature of *Arfrp1*$^{ad-/-}$ mice was significantly re-

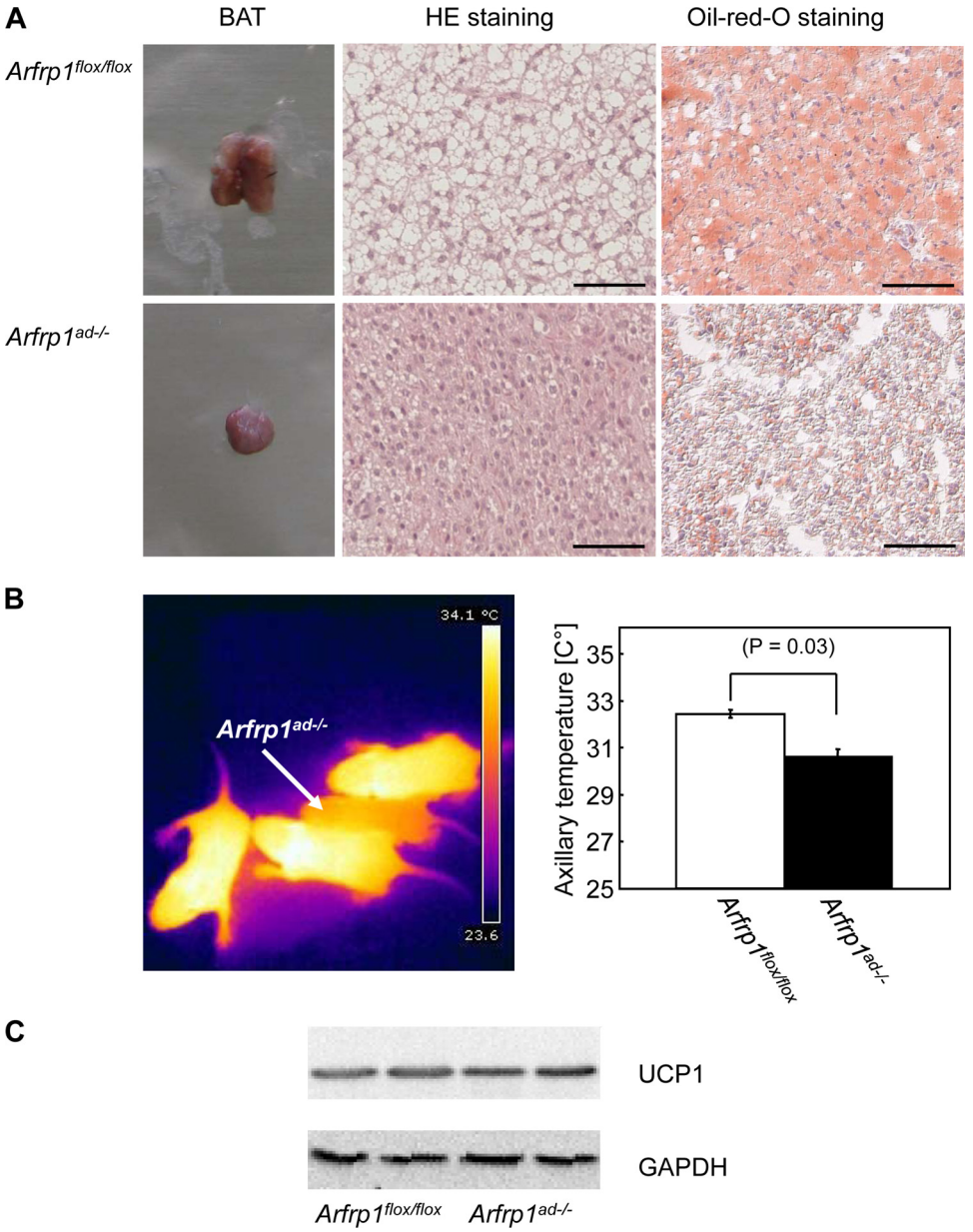


FIG. 4. Reduced size and lipid content of BAT and lower body temperature of *Arfrp1*$^{ad-/-}$ mice. (A) Size, histology, and lipid content as detected by HE and oil Red O staining of BAT of *Arfrp1*$^{flox/flox}$ and *Arfrp1*$^{ad-/-}$ mice at the age of 7 days. Bars, 50 μm. (B) Body temperature of 7-day-old mice was measured by thermographic monitoring with a noncontact thermometer (FLIR Systems i 50). Images of mice taken by the integrated camera (left). Quantification of the axillary body temperature of 7-day-old *Arfrp1*$^{flox/flox}$ and *Arfrp1*$^{ad-/-}$ mice (right). Values are mean ± SEM of 7 to 8 animals per group. (C) Lysates of BAT of 7-day-old *Arfrp1*$^{flox/flox}$ and *Arfrp1*$^{ad-/-}$ mice were analyzed by Western blotting with an anti-UCP1 antibody.

duced by 1.84°C (Fig. 4B). However, differences in body temperature cannot be explained by reduced UCP1 expression because both *Ucp1* mRNA (Fig. 3B) and UCP1 protein levels (Fig. 4C) were not altered in *Arfrp1*$^{ad-/-}$ mice. In addition to the lower body temperature, we detected a significant reduction of blood glucose levels (*Arfrp1*$^{flox/flox}$ mice, 140 ± 24; *Arfrp1*$^{ad-/-}$ mice, 88 ± 33 mg/dl; $P = 0.002$), which might participate in the early death of the *Arfrp1*$^{ad-/-}$ mice.

***Arfrp1* ablation does not impair triglyceride synthesis.** The lipid content extracted from total BAT from control and *Arfrp1*$^{ad-/-}$ mice was reduced in *Arfrp1*$^{ad-/-}$ mice (*Arfrp1*$^{flox/flox}$, 788.75 ± 90.7; and *Arfrp1*$^{ad-/-}$, 367.33 ± 39.8 μg/total BAT of 7-day-old mice). In order to test whether triglyceride synthesis is impaired in *Arfrp1*$^{ad-/-}$ mice due to a defect of a glycerol acyltransferase, we analyzed the lipid composition of BAT of 7-day-old mice by HPLC. We did not detect significant differences in the lipid profiles of *Arfrp1*$^{ad-/-}$ and *Arfrp1*$^{flox/flox}$ mice (Fig. 5A). Additionally, gas chromatography analysis of fatty acid composition demonstrated no alterations in *Arfrp1*$^{ad-/-}$ BAT (Fig. 5B). Therefore, trig-

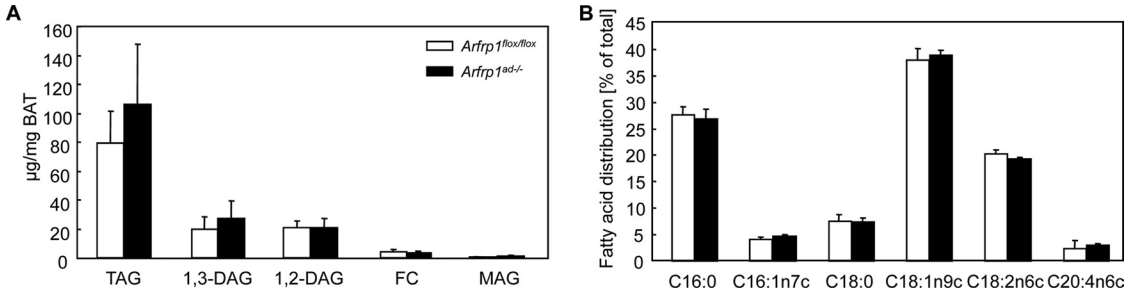


FIG. 5. Proportion of lipids in BAT of *Arfrp1*$^{flox/flox}$ and *Arfrp1*$^{ad-/-}$ mice. Total lipids were extracted from BAT of 7-day-old *Arfrp1*$^{flox/flox}$ and *Arfrp1*$^{ad-/-}$ mice and triacylglycerol (TAG), diacylglycerol (DAG), free cholesterol (FC), and monoacylglcerol (MAG) levels (A), as well as the composition of fatty acids (B), were measured. Values are mean + SEM of 7 to 8 animals per group.

lyceride synthesis in adipocytes is not disrupted in the absence of *Arfrp1*.

**Altered LD size and formation in BAT of *Arfrp1*$^{ad-/-}$ mice.** In order to investigate the structural differences between BATs from *Arfrp1*$^{flox/flox}$ and *Arfrp1*$^{ad-/-}$ mice, we performed electron microscopy. The LDs of *Arfrp1*$^{ad-/-}$ BAT are much smaller than those of control mice, as the overview shown in Fig. 6A (left) demonstrates. Quantification of the number and

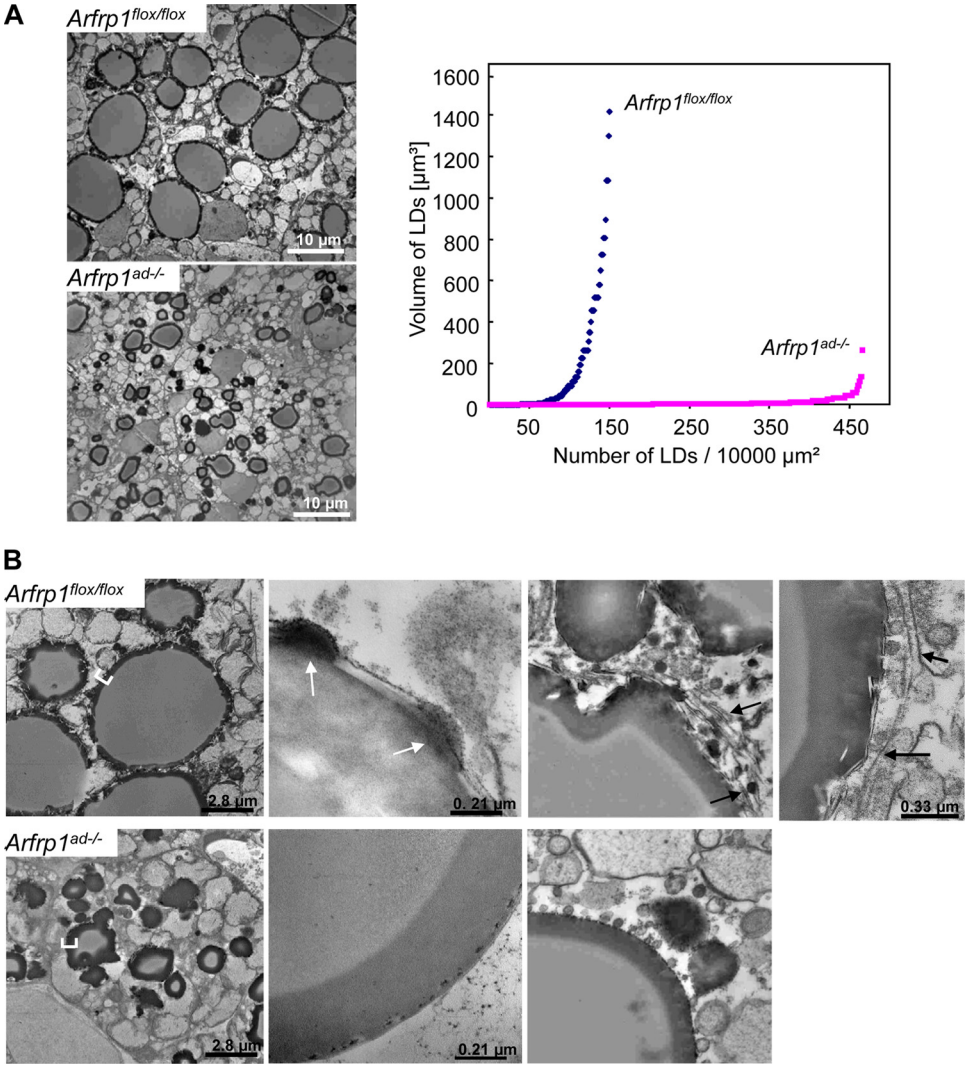


FIG. 6. Reduced size and defective fusion of lipid droplets in BAT of *Arfrp1*$^{ad-/-}$ mice. (A) Ultrastructural analysis of BAT of 7-day-old *Arfrp1*$^{flox/flox}$ and *Arfrp1*$^{ad-/-}$ mice. Electron microscopic overview of ultrathin sections of BAT of 7-day-old *Arfrp1*$^{flox/flox}$ and *Arfrp1*$^{ad-/-}$ mice (left) and quantification and calculation of the number and volume of LDs (right). (B) Sections of BAT analyzed by electron microscopy at higher magnifications (white arrows indicate association of electron-dense droplets with large LD; black arrows indicate membranes which might represent extensions of ER).

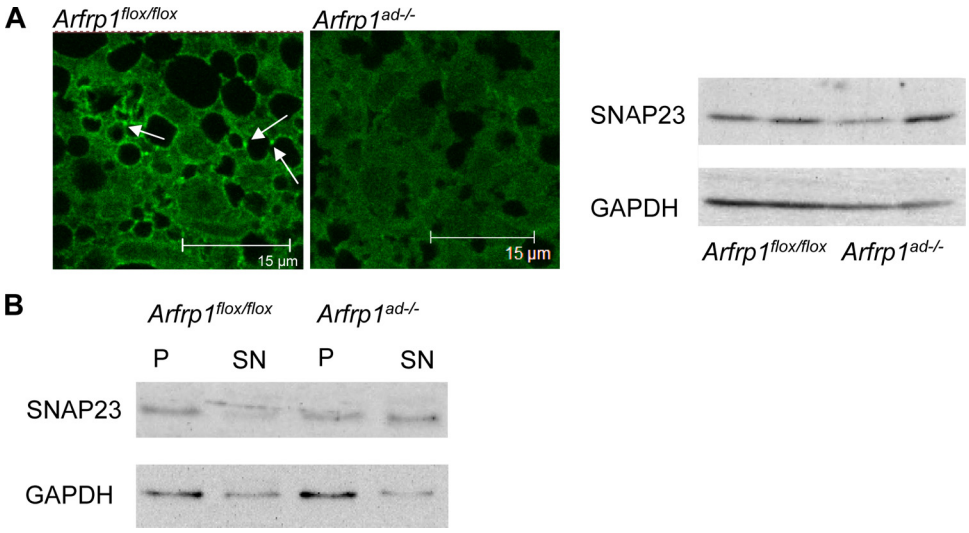


FIG. 7. Altered localization of SNAP23 in *Arfrp1*$^{ad-/-}$ mice. (A) Immunohistochemical staining of SNAP23 in BAT sections of 7-day-old *Arfrp1*$^{flox/flox}$ and *Arfrp1*$^{ad-/-}$ mice (left; white arrows depict SNAP23 associated at lipid droplets). Western blots of BAT lysates stained with the anti-SNAP23 antibody. (B) Detection of SNAP23 in total membranes (P) and the cytosol (SN) of homogenized BAT of 7-day-old *Arfrp1*$^{flox/flox}$ and *Arfrp1*$^{ad-/-}$ mice by Western blotting.

calculation of the volume of the droplets (Fig. 6A, right) indicate that *Arfrp1*$^{ad-/-}$ adipocytes contain more droplets than *Arfrp1*$^{flox/flox}$ adipocytes, with a markedly reduced volume. We counted 467 LDs per 10,000 $\mu m^2$ in specimen of *Arfrp1*$^{ad-/-}$ and 150 in *Arfrp1*$^{flox/flox}$ adipocytes. LDs of *Arfrp1*$^{ad-/-}$ cells were much smaller than those of control cells (diameter of 1.9 ± 1.1 versus 4.5 ± 3.6 μm). The smallest LDs had a diameter of 0.4 μm in both genotypes, whereas the biggest LDs were measured in *Arfrp1*$^{flox/flox}$ adipocytes, with a diameter of 13.9 μm, and in *Arfrp1*$^{ad-/-}$ cells, with a diameter of 8 μm.

An additional striking finding was the alteration of the LD organization in specimen of *Arfrp1*$^{ad-/-}$ BAT. The droplets showed an irregular shape and were not rounded like those in the controls (Fig. 6B, left). The electron-opaque layer in the periphery of the LDs had a different shape; it was broad and smooth in *Arfrp1*$^{ad-/-}$ cells, whereas it was narrow and rough in control adipocytes (Fig. 6B, left). At higher magnification, we observed an association of electron-dense droplets (white arrows in Fig. 6B, top middle) with the large LDs in *Arfrp1*$^{flox/flox}$ cells, contributing to the appearance of a roughly structured surface of the large LDs in control mice, whereas the surface of *Arfrp1*$^{ad-/-}$ droplets appeared smooth. In control specimen, small droplets are interconnected by electron-transparent membranous structures located on the surface of lipid storage droplets (black arrows in Fig. 6B, right). These membranes might represent extensions of the ER (black arrows in Fig. 6B, top right) which interconnect the large LD surface with small adjacent LDs. In contrast, small lipid-containing particles, not organized in membranes, associate with LDs in *Arfrp1*$^{ad-/-}$ adipocytes (Fig. 6B, bottom right).

As recent data suggested that SNAP23 is required for LD assembly (6), we stained sections of BAT from 7-day-old *Arfrp1*$^{ad-/-}$ mice with an anti-SNAP23 antibody. Unlike the majority of SNAREs, SNAP23 has no transmembrane domain and cycles between cytosol and membrane. We detected SNAP23 predominantly in the cytosol and at the cell surface (Fig. 7A) in BAT of the null mutant, whereas SNAP23 associated with small LDs in control specimen (white arrows in Fig. 7A). However, the total levels of SNAP23 protein in lysates did not differ between both genotypes (Fig. 7A, right). In addition, we homogenized BAT of control and knockout mice and separated membranes and cytosol by centrifugation in order to analyze both fractions by Western blotting. These results confirm the observation of the immunohistochemical study and indicate that the level of cytosolic SNAP23 is higher in *Arfrp1*$^{ad-/-}$ BAT than in *Arfrp1*$^{flox/flox}$ BAT (Fig. 7B).

In order to test whether the reduced lipid droplet size of *Arfrp1*$^{ad-/-}$ adipocytes is associated with an alteration of lipid droplet protein composition, we stained sections of BAT of 7-day-old mice with specific antibodies for perilipin, ADRP, TIP47, and Rab18. Perilipin coats the large lipid droplets in *Arfrp1*$^{flox/flox}$ mice (Fig. 8A, top left), whereas it is located on the surface of the small droplets in *Arfrp1*$^{ad-/-}$ adipocytes (Fig. 8A, bottom left). ADRP and TIP47 were nearly undetectable in BAT sections of both *Arfrp1*$^{flox/flox}$ and *Arfrp1*$^{ad-/-}$ mice. They appeared to be associated predominantly with small LD and therefore showed a slightly more intensive signal in *Arfrp1*$^{ad-/-}$ samples. Rab18, which is known to associate with LD when lipolysis is induced (28, 29), shows a more intensive staining in specimen of *Arfrp1*$^{ad-/-}$ mice. We also analyzed the levels of perilipin and other prominent lipid droplet proteins, such as caveolin 1 and 2, in lysates of BAT from 7-day-old *Arfrp1*$^{flox/flox}$ and *Arfrp1*$^{ad-/-}$ mice but did not find differences in their expression levels (Fig. 8B).

**Impaired LD formation in MEFs lacking *Arfrp1*.** To further characterize the LD formation in the absence of *Arfrp1*, we used MEFs of *Arfrp1*$^{+/+}$ and *Arfrp1*$^{flox/flox}$ embryos infected with Cre-expressing adenovirus for *Arfrp1* deletion. Cre expression resulted in a 65 to 69% inhibition of *Arfrp1* expression in *Arfrp1*$^{flox/flox}$ MEFs, whereas no alterations were obtained in virus-infected *Arfrp1*$^{+/+}$ MEFs. In order to identify cells which lack *Arfrp1*, we stained ARL1, which dissociates from Golgi

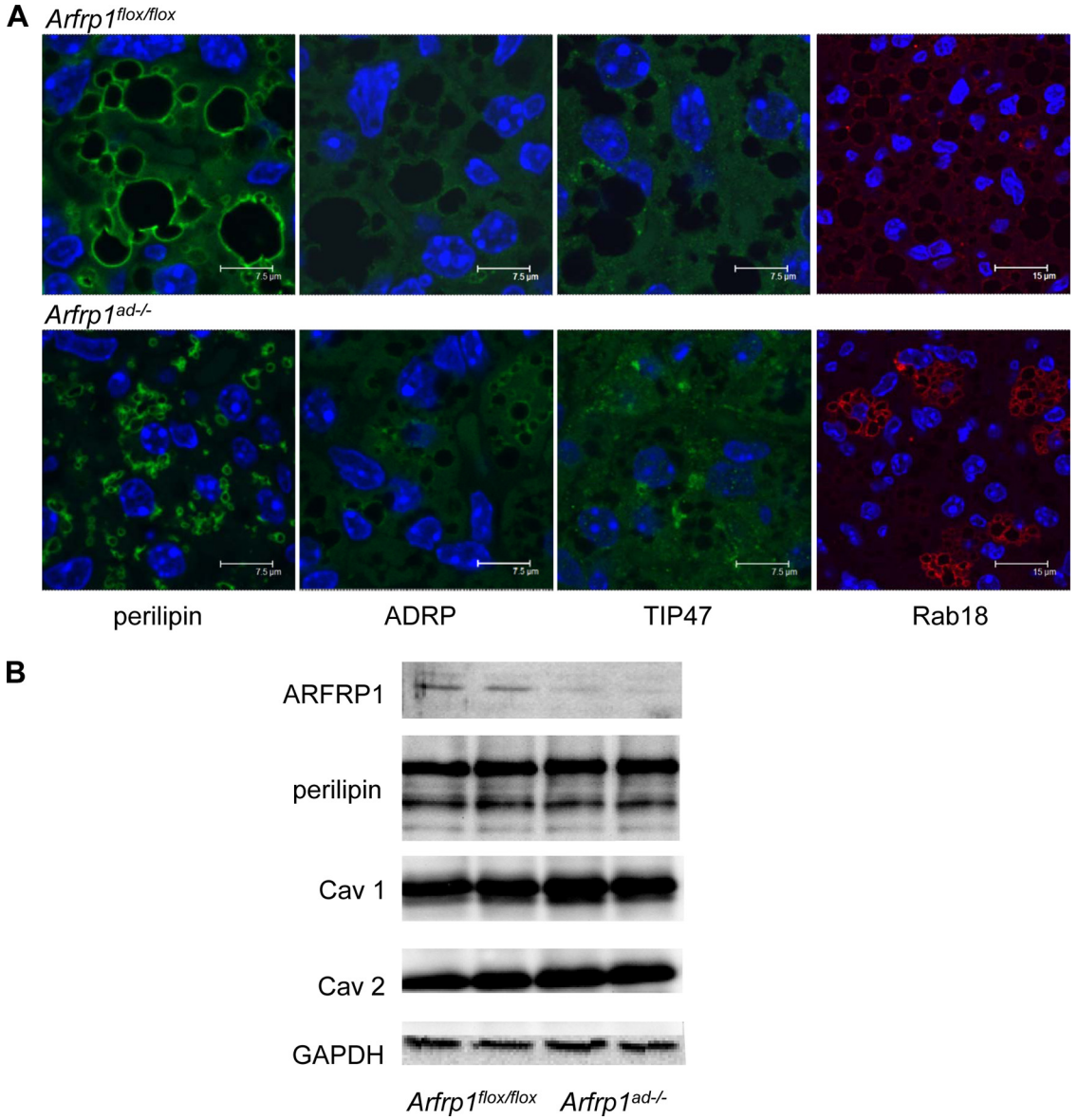


FIG. 8. Investigation of LD proteins in *Arfrp1*$^{flox/flox}$ and *Arfrp1*$^{ad-/-}$ BAT. (A) Immunohistochemical detection of perilipin, ADRP, TIP47, and Rab18 in *Arfrp1*$^{flox/flox}$ and *Arfrp1*$^{ad-/-}$ adipocytes. Paraffin sections of BAT from 7-day-old *Arfrp1*$^{flox/flox}$ and *Arfrp1*$^{ad-/-}$ mice were stained with the indicated antibodies in combination with an Alexa-488- or an Alexa-546-conjugated secondary antibody and analyzed by confocal laser scanning microscopy. (B) Expression of LD proteins perilipin, caveolin 1 (Cav1), and caveolin 2 (Cav2) detected in lysates of BAT of 7-day-old mice by Western blotting with indicated antibodies. GAPDH was detected as loading control.

membranes in the absence of *Arfrp1* (5). When Cre virus-treated *Arfrp1*$^{+/+}$ cells were incubated with 2 mM oleate for 48 h, LDs accumulated within the cell, as detected by staining with Bodipy (Fig. 9). The same picture was observed with oleate-loaded, uninfected *Arfrp1*$^{flox/flox}$ cells. In contrast, LD formation was markedly impaired in cells lacking *Arfrp1* due to Cre-mediated recombination (Fig. 9, bottom).

**Reduced *Arfrp1* expression enhances lipolysis in adipocytes.** We next tested whether the lipolysis was elevated in *Arfrp1*$^{ad-/-}$ adipocytes and thus also responsible for the reduced fat mass and the lipodystrophic phenotype of *Arfrp1*$^{ad-/-}$ mice. Two adipocyte lipases, HSL and ATGL, are important for controlling lipolysis. Induction of lipolysis results in the protein kinase A-mediated phosphorylation of HSL (43). As shown in Fig. 10A, we detected elevated amounts of phosphorylated HSL and slightly higher levels of ATGL in lysates of *Arfrp1*$^{ad-/-}$ BAT, supporting the assumption that lipolysis is enhanced in BAT in the absence of *Arfrp1*. In addition, both lipases predominantly associated with the small LDs of *Arfrp1*$^{ad-/-}$ BAT (Fig. 10A, right).

Since mice with strong reduction of *Arfrp1* expression did not survive the first 3 weeks, it was impossible to measure lipolysis in isolated adipocytes of *Arfrp1*$^{ad-/-}$ mice. We therefore inhibited *Arfrp1* expression in 3T3-L1 adipocytes (Fig. 10B). Here we also detected ATGL associated with LDs, as detected by yellow signals in the merged pictures shown in Fig. 10B (right bottom) after downregulation of *Arfrp1*. Basal and

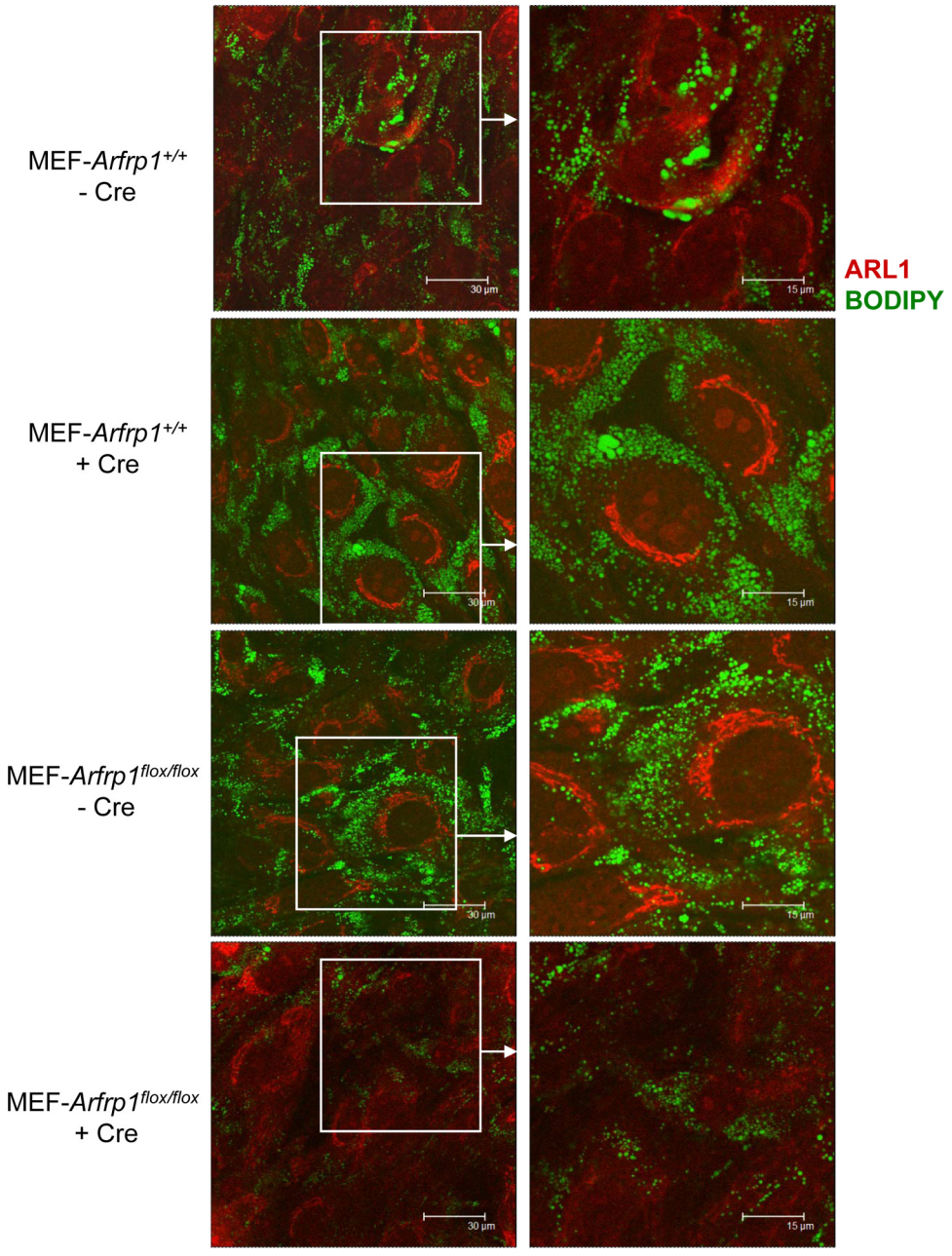


FIG. 9. Impaired LD formation in MEFs lacking *Arfrp1*. MEFs of *Arfrp1*$^{+/+}$ and *Arfrp1*$^{flox/flox}$ embryos were infected with Cre-expressing adenovirus and incubated with oleate for 2 days. Cells were stained with an anti-ARL1 antibody in order to identify cells with deleted *Arfrp1*. LDs were visualized by staining with Bodipy.

insulin-stimulated palmitate uptake was not different between control and siRNA-transfected adipocytes (Fig. 10C, left). However, basal lipolysis was significantly ($P = 0.00002$) increased in *Arfrp1* knockdown 3T3-L1 adipocytes by about 100%, whereas isoproterenol-stimulated lipolysis was not altered (Fig. 10C, right).

## DISCUSSION

The striking phenotype of mice lacking *Arfrp1* in adipose tissues (*Arfrp1*$^{ad-/-}$ mice) was an almost complete absence or marked reduction of lipid storage in white or brown adipocytes, respectively, due to defective interaction and growth of LDs. It has been generally accepted that LDs derive from the ER by incorporating a growing triacylglycerol core between the leaflets of the bilayer (26, 28, 33). However, recently several proteomic and functional genomic screens were performed with yeast (1), mammalian tissue culture (7, 15, 23, 42), and *Drosophila* cells (3, 4, 16) in order to find new proteins and pathways involved in LD biology. Several proteins were identified as being associated with LDs interconnecting them with various cellular compartments (44, 45). Recently, two groups

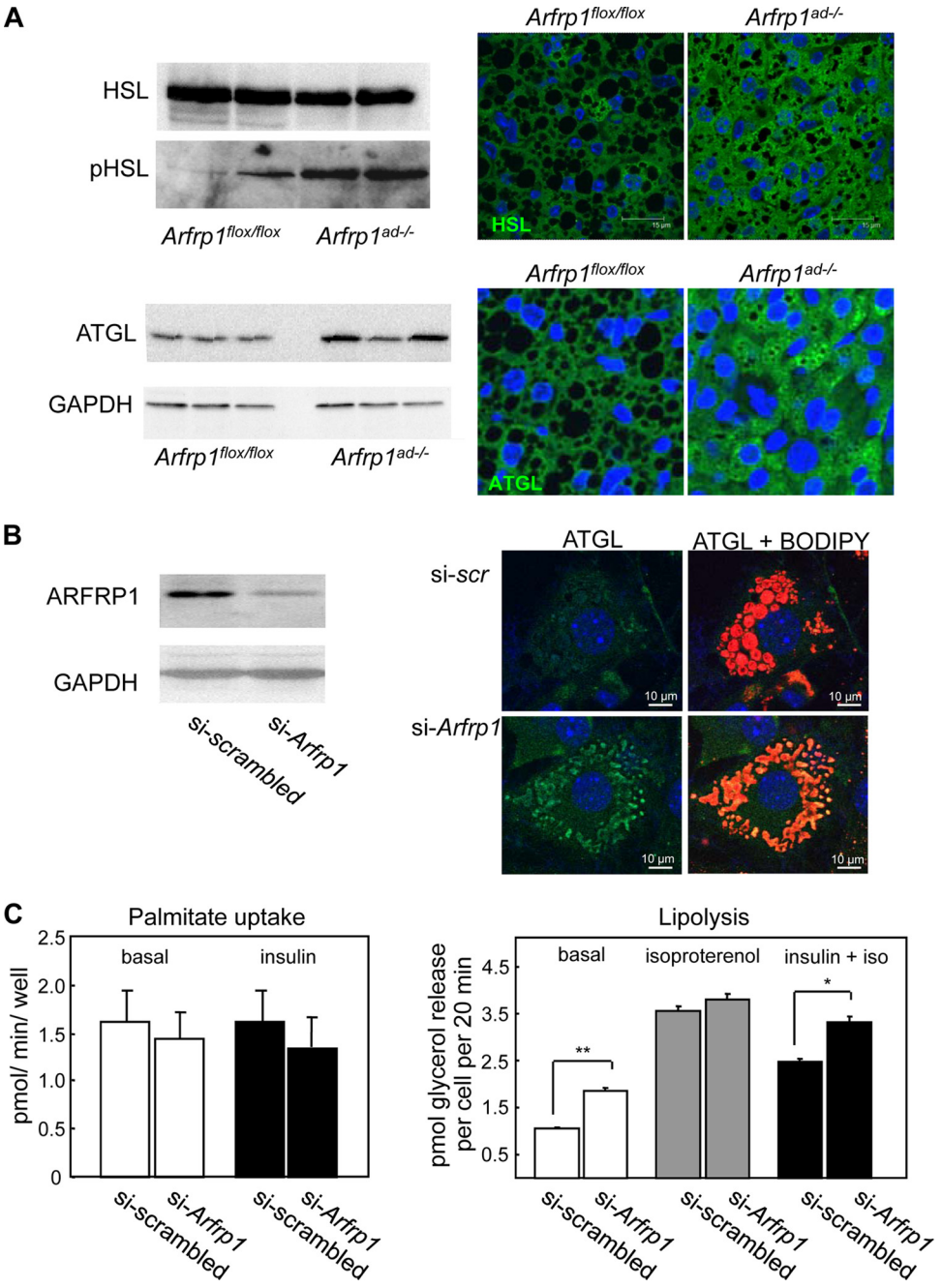


FIG. 10. Enhanced lipolysis in *Arfrp1*$^{ad-/-}$ BAT and in 3T3-L1 adipocytes after downregulation of *Arfrp1*. (A) Levels of HSL, phosphorylated HSL (pHSL), and ATGL were detected by Western blotting with lysates (left) and by immunostaining with specific antibodies on sections of BAT from 7-day-old *Arfrp1*$^{flox/flox}$ and *Arfrp1*$^{ad-/-}$ animals (right). (B) *Arfrp1* expression was suppressed in 3T3-L1 adipocytes by siRNA and analyzed by Western blotting with an anti-ARFRP1 specific antibody (left). Immunocytochemical detection of ATGL costained with Bodipy (right). (C) Palmitate uptake (left) was measured under basal and insulin-stimulated conditions. Lipolysis (right) was measured under basal conditions and after stimulation with isoproterenol (iso) and insulin together with isoproterenol in scrambled and si-*Arfrp1*transfected 3T3-L1 adipocytes (*, $P = 0.00117$; **, $P = 0.00002$).

discovered that ARF1-COPI vesicular transport proteins, involved in vesicle formation at the Golgi membrane, regulate LD morphology and lipid utilization (4, 16). Therefore, the identification of the role of ARFRP1 in mediating LD growth might fill a gap in knowledge of protein/membrane transport between the Golgi membrane and the LD.

Ultrastructural analysis of the growing BAT of 7-day-old control mice demonstrated that longitudinal electron transparent structures associate with small LDs (Fig. 4B). These structures are suggested to represent a subcompartment of the ER (33), mediating connection of small lipid-loaded particles with larger lipid storage droplets. Since we rarely observed such interactions in adipocytes of *Arfrp1*$^{ad-/-}$ mice, we conclude that LD size in *Arfrp1*$^{ad-/-}$ adipocytes is restricted due to a

defective transfer of newly synthesized LDs to larger storage droplets.

How does ARFRP1 modify LD size? (i) Boström et al. (6) demonstrated that the soluble *N*-ethylmaleimide-sensitive factor adaptor protein receptor, SNAP23, is required for the fusion process of LDs. Actually, we determined a predominantly cytosolic localization of SNAP23 in BAT sections of *Arfrp1*$^{ad-/-}$ mice, in contrast to an association with several LDs in *Arfrp*$^{flox/flox}$ adipocytes (Fig. 4C). Therefore, it is conceivable that ARFRP1 acts upstream of SNAP23 and is thereby required for fusion of LDs. (ii) The ARF1-COPI machinery modifies lipid homeostasis by regulating PAT protein composition at the LD and promoting lipolysis via targeting of ATGL to the droplet (4, 40). Since ARFRP1 interacts with the ARF-specific nucleotide exchange factor mSec7/cytohesin in a GTP-dependent manner (35) and inhibits ARF1 activity, one could speculate that lipolysis is elevated in *Arfrp1*$^{ad-/-}$ BAT due to an altered ARF1-COPI machinery. However, the exchange factor regulating COPI in ER-Golgi trafficking is GBF1 and not cytohesin, and there is no evidence for cytohesins acting at the Golgi membrane under normal conditions. In addition, depletion of *Arfrp1* leads to increased amounts of ATGL on LDs, as it is also observed after activation of COPI. Therefore, we conclude that the interaction of ARFRP1 with cytohesin and the resulting inhibition of ARF1 activity cannot be responsible for the observed phenotype. (iii) Several Rab GTPases (Rab5, Rab7, Rab11, and Rab18), essential regulators of vesicular traffic, associate with LDs (2, 25). In a screen of *Drosophila* S2 cells, Rab proteins were identified to bind to GRIP domain proteins (39), which are recruited via binding to ARL1 to *trans*-Golgi membranes in the presence of activated ARFRP1 (31, 38, 48). Therefore, it is also likely that ARFRP1 alters Rab targeting. Actually, we detected more LDs in which Rab18 associated with LD in *Arfrp1*$^{ad-/-}$ BAT, presumably as a secondary effect of elevated lipolysis. Since Rab18 was not identified to interact with GRIP proteins (39), we conclude that the altered Rab18 localization is not a consequence of a defective ARFRP-ARL1-GRIP pathway.

Here we demonstrate that deletion of *Arfrp1* affects two processes in adipocytes, LD growth presumably via fusion events and lipolysis. We assume that active ARFRP1 regulates the correct targeting of SNAP23 to the LD and the dissociation of ATGL from the LD. Thereby, *Arfrp1*$^{ad-/-}$ mice suffer from secondary effects, such as reduced body temperature (Fig. 2). Thermogenesis in BAT generates heat through the uncoupling of mitochondrial β-oxidation from ATP production (37). The principal energy source for this process is fatty acids which are either synthesized *de novo* in BAT or imported from the circulation. Therefore, maintenance of adequate stores of triacylglycerol is essential for normal BAT function. Temperature homeostasis is disrupted in *Arfrp1*$^{ad-/-}$ mice (Fig. 2) because the marked reduction of the BAT depots finally results in a total reduction of UCP1. This, together with a lower capacity to dissipate energy as heat from the reduced fat stores, appears to be responsible for the defective thermogenesis of the *Arfrp1*$^{ad-/-}$ mice. This is similar to the phenotype of *FATP1*$^{-/-}$ mice which exhibit reduced basal fatty acid uptake and smaller LDs in BAT and fail to defend their core body temperature at 4°C (46).

The present data demonstrate that fat-specific deletion of the GTPase ARFRP1 severely compromises lipid storage in fat cells, presumably due to defective LD enlargement and enhanced lipolysis.

## ACKNOWLEDGMENTS

This work was supported by the Deutsche Forschungsgemeinschaft (Schu 750/5-2 and Schu 750/5-3) and the European Community's FP7 PREPROBEDIA (grant 201681).

We are grateful to Ronald M. Evans, Howard Hughes Medical Institute, The Salk Institute, La Jolla, CA, for providing the *Cre-ap2* mouse and to Richard A. Kahn, Department of Biochemistry, Emory University School of Medicine, Atlanta, GA, for critical reading of the manuscript and helpful discussions. The skillful technical assistance of M. Fobker, W. Hanekamp, E. Meyer, B. Rischke, K. Schlattmann, A. Seelig, and D. Ziomek is gratefully acknowledged.

Conflict of interest statement: none declared.

## REFERENCES

1. **Athenstaedt, K., D. Zweytick, A. Jandrositz, S. D. Kohlwein, and G. Daum.** 1999. Identification and characterization of major lipid particle proteins of the yeast *Saccharomyces cerevisiae*. J. Bacteriol. **181:**6441–6448.
2. **Bartz, R., J. K. Zehmer, M. Zhu, Y. Chen, G. Serrero, Y. Zhao, and P. Liu.** 2007. Dynamic activity of lipid droplets: protein phosphorylation and GTP-mediated protein translocation. J. Proteome Res. **6:**3256–3265.
3. **Beller, M., D. Riedel, L. Jänsch, G. Dieterich, J. Wehland, H. Jäckle, and R. P. Kühnlein.** 2006. Characterization of the Drosophila lipid droplet subproteome. Mol. Cell. Proteomics **5:**1082–1094.
4. **Beller, M., C. Sztalryd, N. Southall, M. Bell, H. Jäckle, D. S. Auld, and B. Oliver.** 2008. COPI complex is a regulator of lipid homeostasis. PLoS Biol. **6:**e292.
5. **Blüher, M., M. D. Michael, O. D Peroni, K. Ueki, N. Carter, B. B. Kahn, and C. R. Kahn.** 2002. Adipose tissue selective insulin receptor knockout protects against obesity and obesity-related glucose intolerance. Dev. Cell **3:**25–38.
6. **Boström, P., L. Andersson, M. Rutberg, J. Perman, U. Lidberg, B. R. Johansson, J. Fernandez-Rodriguez, J. Ericson, T. Nilsson, J. Borén, and S. O. Olofsson.** 2007. SNARE proteins mediate fusion between cytosolic lipid droplets and are implicated in insulin sensitivity. Nat. Cell Biol. **9:**1286–1293.
7. **Brasaemle, D. L., G. Dolios, L. Shapiro, and R. Wang.** 2004. Proteomic analysis of proteins associated with lipid droplets of basal and lipolytically stimulated 3T3-L1 adipocytes. J. Biol. Chem. **279:**46835–46842.
8. **Brasaemle, D. L., D. M. Levin, D. C. Adler-Wailes, and C. Londos.** 2000. The lipolytic stimulation of 3T3-L1 adipocytes promotes the translocation of hormone-sensitive lipase to the surfaces of lipid storage droplets. Biochim. Biophys. Acta **1483:**251–262.
9. **Brown, D. A.** 2001. Lipid droplets: proteins floating on a pool of fat. Curr. Biol. **11:**446–449.
10. **Buchmann, J., C. Meyer, S. Neschen, R. Augustin, K. Schmolz, R. Kluge, H. Al-Hasani, H. Jurgens, K. Eulenberg, R. Wehr, C. Dohrmann, H. G. Joost, and A. Schürmann.** 2007. Ablation of the cholesterol transporter adenosine triphosphate-binding cassette transporter G1 reduces adipose cell size and protects against diet-induced obesity. Endocrinology **148:**1561–1573.
11. **Butovich, I. A., F. Uchiyama, M. A. Di Pascuale, and J. P. McCulley.** 2007. Liquid chromatography-mass spectrometric analysis of lipids present in human meibomian gland secretions. Lipids **42:**765–776.
12. **Chadt, A., K. Leicht, A. Deshmukh, L. Q. Jiang, S. Scherneck, U. Bernhardt, T. Dreja, H. Vogel, K. Schmolz, R. Kluge, J. R. Zierath, C. Hultschig, R. C. Hoeben, A. Schürmann, H. G. Joost, and H. Al-Hasani.** 2008. Tbc1d1 mutation in lean mouse strain confers leanness and protects from diet-induced obesity. Nat. Genet. **40:**1354–1359.
13. **Folch, J., M. Lees, and G. H. Sloane Stanley.** 1957. A simple method for the isolation and purification of total lipides from animal tissues. J. Biol. Chem. **226:**497–509.
14. **Frayn, K. N., and P. F. Maycock.** 1980. Skeletal muscle triacylglycerol in the rat: methods for sampling and measurement, and studies of biological variability. J. Lipid Res. **21:**139–144.
15. **Fujimoto, Y., H. Itabe, J. Sakai, M. Makita, J. Noda, M. Mori, Y. Higashi, S. Kojima, and T. Takano.** 2004. Identification of major proteins in the lipid droplet-enriched fraction isolated from the human hepatocyte cell line HuH7. Biochim. Biophys. Acta **1644:**47–59.
16. **Guo, Y., T. C. Walther, M. Rao, N. Stuurman, G. Goshima, K. Terayama, J. S. Wong, R. D. Vale, P. Walter, and R. V. Farese.** 2008. Functional genomic screen reveals genes involved in lipid-droplet formation and utilization. Nature **453:**657–661.
17. **He, W., Y. Barak, A. Hevener, P. Olson, D. Liao, J. Le, M. Nelson, E. Ong, J. M. Olefsky, and R. M. Evans.** 2003. Adipose-specific peroxisome proliferator-activated receptor gamma knockout causes insulin resistance in fat and liver but not in muscle. Proc. Natl. Acad. Sci. U. S. A. **100:**15712–15717.
18. **Kahn, R. A.** 2003. ARF family GTPases. Kluwer Academic Publishers, Dordrecht, The Netherlands.

19. **Kahn, R. A., J. Cherfils, M. Elias, R. C. Lovering, S. Munro, and A. Schürmann.** 2006. Nomenclature for the human Arf family of GTP-binding proteins: ARF, ARL, and SAR proteins. J. Cell Biol. **172:**645–650.
20. **Kratz, M., P. Cullen, F. Kannenberg, A. Kassner, M. Fobker, P. M. Abuja, G. Assmann, and U. Wahrburg.** 2002. Effects of dietary fatty acids on the composition and oxidizability of low-density lipoprotein. Eur. J. Clin. Nutr. **56:**72–81.
21. **Kuerschner, L., C. Moessinger, and C. Thiel.** 2008. Imaging of lipid biosynthesis: how a neutral lipid enters lipid droplets. Traffic **9:**338–352.
22. **Liu, P., R. Bartz, J. K. Zehmer, Y. S. Ying, M. Zhu, G. Serrero, and R. G. Anderson.** 2007. Rab-regulated interaction of early endosomes with lipid droplets. Biochim. Biophys. Acta **1773:**784–793.
23. **Liu, P., Y. Ying, Y. Zhao, D. I. Mundy, M. Zhu, and R. G. Anderson.** 2004. Chinese hamster ovary K2 cell lipid droplets appear to be metabolic organelles involved in membrane traffic. J. Biol. Chem. **279:**3787–3792.
24. **Marchesan, D., M. Rutberg, L. Andersson, L. Asp, T. Larsson, J. Borén, B. R. Johansson, and S. O. Olofsson.** 2003. A phospholipase D-dependent process forms lipid droplets containing caveolin, adipocyte differentiation-related protein, and vimentin in a cell-free system. J. Biol. Chem. **278:**27293–27300.
25. **Martin, S., K. Driessen, S. J. Nixon, M. Zerial, and R. G. Parton.** 2005. Regulated localization of Rab18 to lipid droplets: effects of lipolytic stimulation and inhibition of lipid droplet catabolism. J. Biol. Chem. **280:**42325–42335.
26. **Martin, S., and R. G. Parton.** 2008. Characterization of Rab18, a lipid droplet-associated small GTPase. Methods Enzymol. **438:**109–129.
27. **Mueller, A. G., M. Moser, R. Kluge, S. Leder, M. Blum, R. Büttner, H. G. Joost, and A. Schürmann.** 2002. Embryonic lethality caused by apoptosis during gastrulation in mice lacking the gene of the ADP-ribosylation factor-related protein 1. Mol. Cell. Biol. **22:**1488–1494.
28. **Murphy, D. J.** 2001. The biogenesis and functions of lipid bodies in animals, plants and microorganisms. Prog. Lipid Res. **40:**325–438.
29. **Olofsson, S. O., P. Boström, L. Andersson, M. Rutberg, M. Levin, J. Perman, and J. Borén.** 2008. Triglyceride containing lipid droplets and lipid droplet-associated proteins. Curr. Opin. Lipidol. **19:**441–447.
30. **Ozeki, S., J. Cheng, K. Tauchi-Sato, N. Hatano, H. Taniguchi, and T. Fujimoto.** 2005. Rab18 localizes to lipid droplets and induces their close apposition to the endoplasmic reticulum-derived membrane. J. Cell Sci. **118:**2601–2611.
31. **Panic, B., J. R. Whyte, and S. Munro.** 2003. The ARF-like GTPases Arl1p and Arl3p act in a pathway that interacts with vesicle-tethering factors at the Golgi apparatus. Curr. Biol. **13:**405–410.
32. **Robenek, H., I. Buers, O. Hofnagel, M. J. Robenek, D. Troyer, and N. J. Severs.** 2009. Compartmentalization of proteins in lipid droplet biogenesis. Biochim. Biophys. Acta **1791:**408–418.
33. **Robenek, H., O. Hofnagel, I. Buers, M. J. Robenek, D. Troyer, and N. J. Severs.** 2006. Adipophilin-enriched domains in the ER membrane are sites of lipid droplet biogenesis. Adipophilin-enriched domains in the ER membrane are sites of lipid droplet biogenesis. J. Cell Sci. **119:**4215–4224.
34. **Schürmann, A., S. Massmann, and H. G. Joost.** 1995. ARP is a plasma membrane-associated Ras-related GTPase with remote similarity to the family of ADP-ribosylation factors. J. Biol. Chem. **270:**30657–30663.
35. **Schürmann, A., M. Schmidt, M. Asmus, S. Bayer, F. Fliegert, S. Koling, S. Massmann, C. Schilf, M. C. Subauste, M. Voss, K. H. Jakobs, and H. G. Joost.** 1999. The ADP-ribosylation factor (ARF)-related GTPase ARF-related protein binds to the ARF-specific guanine nucleotide exchange factor cytohesin and inhibits the ARF-dependent activation of phospholipase D. J. Biol. Chem. **274:**9744–9751.
36. **Seligman, A. M., H. L. Wasserkrug, and J. S. Hanker.** 1966. A new staining method (OTO) for enhancing contrast of lipid containing membranes and droplets in osmium tetroxide-fixed tissue with osmiophilic thiocarboxyhydrazide (TCH). J. Cell Biol. **30:**424–432.
37. **Sell, H., Y. Deshaies, and D. Richard.** 2004. The brown adipocyte: update on its metabolic role. Int. J. Biochem. Cell Biol. **36:**2098–2104.
38. **Setty, S. R., M. E. Shin, A. Yoshino, M. S. Marks, and C. G. Burd.** 2003. Golgi recruitment of GRIP domain proteins by Arf-like GTPase 1 is regulated by Arf-like GTPase 3. Curr. Biol. **13:**401–404.
39. **Sinka, R., A. K. Gillingham, V. Kondylis, and S. Munro.** 2008. Golgi coiled-coil proteins contain multiple binding sites for Rab family G proteins. J. Cell Biol. **183:**607–615.
40. **Soni, K. G., G. A. Mardones, R. Sougrat, E. Smirnova, C. L. Jackson, and J. S. Bonifacino.** 2009. Coatomer-dependent protein delivery to lipid droplets. J. Cell Sci. **122:**1834–1841.
41. **Su, C. L., C. Sztalryd, J. A. Contreras, C. Holm, A. R. Kimmel, and C. Londos.** 2003. Mutational analysis of the hormone-sensitive lipase translocation reaction in adipocytes. J. Biol. Chem. **278:**43615–43619.
42. **Umlauf, E., E. Csaszar, M. Moertelmaier, G. J. Schuetz, R. G. Parton, and R. Prohaska.** 2004. Association of stomatin with lipid bodies. J. Biol. Chem. **279:**23699–23709.
43. **Wang, J., W. J. Shen, S. Patel, K. Harada, and F. B. Kraemer.** 2005. Mutational analysis of the "regulatory module" of hormone-sensitive lipase. Biochemistry **44:**1953–1959.
44. **Welte, M. A., S. Cermelli, J. Griner, A. Viera, Y. Guo, D. H. Kim, J. G. Gindhart, and S. P. Gross.** 2005. Regulation of lipid-droplet transport by the perilipin homolog LSD2. Curr. Biol. **15:**1266–1275.
45. **Wu, C. C., K. E. Howell, M. C. Neville, J. R. Yates III, and J. L. McManaman.** 2000. Proteomics reveal a link between the endoplasmic reticulum and lipid secretory mechanisms in mammary epithelial cells. Electrophoresis **21:**3470–3482.
46. **Wu, Q., M. Kazantzis, H. Doege, A. M. Ortegon, B. Tsang, A. Falcon, and A. Stahl.** 2006. Fatty acid transport protein 1 is required for nonshivering thermogenesis in brown adipose tissue. Diabetes **55:**3229–3237.
47. **Zahn, C., A. Hommel, L. Lu, W. Hong, D. J. Walther, S. Florian, H. G. Joost, and A. Schürmann.** 2006. Knockout of Arfrp1 leads to disruption of ARF-like 1 (ARL1) targeting to the *trans*-Golgi in mouse embryos and HeLa cells. Mol. Membr. Biol. **23:**475–485.
48. **Zahn, C., A. Jaschke, J. Weiske, A. Hommel, D. Hesse, R. Augustin, L. Lu, W. Hong, S. Florian, A. Scheepers, H. G. Joost, O. Huber, and A. Schürmann.** 2008. ADP-ribosylation factor-like GTPase ARFRP1 is required for *trans*-Golgi to plasma membrane trafficking of E-cadherin. J. Biol. Chem. **283:**27179–27188.